

**Role of break-up processes in the fusion of the  $^{12}\text{C} + ^{52}\text{Cr}$  system**F. K. Amanuel,<sup>1,\*</sup> B. Zelalem,<sup>2</sup> A. K. Chaubey,<sup>2</sup> Avinash Agarwal,<sup>3</sup> I. A. Rizvi,<sup>4</sup> Anjana Maheshwari,<sup>4</sup> and Tauseef Ahmed<sup>4</sup><sup>1</sup>*INFN, Laboratori Nazionali di Legnaro, Legnaro (Padova), Italy*<sup>2</sup>*Department of Physics, Addis Ababa University, P.O. Box 1176, Addis Ababa, Ethiopia*<sup>3</sup>*Department of Physics, Bareilly College, Bareilly 243005, India*<sup>4</sup>*Department of Physics, Aligarh Muslim University, Aligarh 202002, India*

(Received 27 September 2010; revised manuscript received 14 June 2011; published 25 August 2011)

We present the results and analysis of our investigation of the role of break-up processes on the fusion of a  $^{12}\text{C}^{6+}$  beam with a  $^{52}\text{Cr}$  target near, at, and above the Coulomb barrier. In this experiment the excitation functions of evaporation residues produced via ( $^{12}\text{C}, 2n$ ), ( $^{12}\text{C}, pxn$ ), ( $^{12}\text{C}, \alpha xn$ ), and ( $^{12}\text{C}, \alpha pxn$ ) channels in a  $^{12}\text{C} + ^{52}\text{Cr}$  reaction were measured at several beam energies ranging from  $\approx 51$  to 87 MeV by employing the recoil catcher technique followed by off-line  $\gamma$ -ray spectrometry. The measured excitation functions were compared with theoretical values obtained using the PACE4 statistical model code. Further, for a ( $^{12}\text{C}, p2n$ ) channel the measured excitation function was compared with the predictions of the ALICE-91 code, which was chosen as it takes into account pre-equilibrium emissions. For non- $\alpha$ -emitting channels, the experimentally measured excitation functions—after correcting them for possible contributions from higher charge isobaric precursor decays—were, in general, found to be in good agreement with theoretical predictions. However, for  $\alpha$ -emitting channels, the measured excitation functions had significantly more production cross sections than what PACE4 predicted. This enhancement may be attributed to incomplete fusion processes. An attempt was made to estimate the incomplete fusion fraction in order to compare the relative importance of complete and incomplete fusion processes. The incomplete fusion fraction was found to be sensitive to the projectile energy and mass asymmetry of the entrance channel. We also discuss the results in terms of the impact of the frozen  $\alpha$ -cluster structure of the  $^{12}\text{C}$  isotope on various fusion reactions.

DOI: [10.1103/PhysRevC.84.024614](https://doi.org/10.1103/PhysRevC.84.024614)

PACS number(s): 25.70.Jj, 25.70.Gh, 25.70.Mn

**I. INTRODUCTION**

Advances in accelerator technology have enabled heavy ions to be used as a projectiles in nuclear reactions. This development has broadened and improved our understanding and knowledge of reaction dynamics and nuclear structures at energies near and above the Coulomb barrier [1–6]. Recent studies report that, not only are both complete fusion (CF) and incomplete fusion (ICF) reactions possible at these energies, the two forms of reactions are, in fact, the most dominant reaction mechanisms [7–10].

In CF reactions, the projectile completely fuses with the target nucleus. The projectile and the target nucleus form a single excited complex system, which may eventually become a fully equilibrated compound nucleus (CN). At later stages, the CN deexcites via the emission of light nuclear particles and/or  $\gamma$  rays. In contrast, in ICF reactions, only a part of the projectile fuses with the target nucleus, leading to the formation of an excited incompletely fused composite system with a mass and/or charge lower than that of the CN [11], while the remaining part escapes in forward cone with approximately the beam velocity. The most common features of ICF reactions are (i) the outgoing particles have a forward peaked angular distribution and an energy spectrum that peaks at beam velocity [12] and (ii) the recoil range distribution of the heavy residues shows low-range components, suggesting incomplete momentum transfer.

Further, pre-equilibrium (PE) emission of nucleons from the composite system before thermalization has also been observed at these energies [1,2,13–16]. Recently, it has also been observed that ICF becomes more and more dominant as the projectile energy increases [17–23]. Moreover, it is now known that CF reactions occur where the angular momentum imparted to the system is less than or equal to  $l_{\text{crit}}$  [24]. In a sharp cutoff approximation, the probability of CF is assumed to be unity for  $l \leq l_{\text{crit}}$  and expected to be zero for  $l > l_{\text{crit}}$  [25,26]; while at relatively higher projectile energies and at finite values of the impact parameters, CF gradually gives way to ICF. It may further be pointed out that the multitude of driving input angular momentum may vary with the projectile energy and/or with the impact parameter. However, there is no a sharp boundary line separating the regions of occurrence of CF and ICF processes: both processes have been observed below and/or above the limiting value of the input angular momentum. A few reports have revealed that ICF can selectively populate high-spin states in the final reaction products at low bombarding energies and can be used as a spectroscopic tool as well [27,28]. In addition, the ICF reactions have a high probability of populating neutron-rich nuclides compared to CF reactions, providing opportunities to study nuclei along the neutron-rich side of the line of stability [29].

Several dynamical models have been proposed to explain the mechanism of ICF reactions. The break-up fusion model of Udagawa and Tamura [30] explained ICF in terms of the break-up of the projectile in the nuclear force field of the target nucleus followed by fusion of one of the fragments

\*kifle@lnl.infn.it

with the target. The model uses the distorted wave Born approximation to evaluate the shapes of the energy spectra and the angular distributions of projectilelike fragments but does not give absolute cross sections, due to the lack of information about the spectroscopic form factors of the continuum states of the product nuclei. The sum rule model of Wilczynski *et al.* [31] assumes that the various ICF channels are localized in the angular momentum space above the critical angular momentum for a CF of the projectile and the target. The model gives cross sections for reaction products arising not only from ICF and quasielastic transfer reactions but also from CF. Other dynamical models, like the exciton model [32], the hot spot model [33], the promptly emitted particles model [34], and the multistep direct reaction model [35] have been proposed to explain ICF dynamics. Apart from the aforementioned dynamical models, Morgenstern *et al.* [36,37] have investigated the mass asymmetry dependence of the ICF contribution. The details of the above models are given in Ref. [38].

Reasonably studies on ICF have been confined to beam energies greater than 10 MeV/nucleon. However, none of the proposed models is able to reproduce the experimental data obtained at energies as low as  $\approx 4$ –8 MeV/nucleon.

Recent experiments have shown significant ICF contributions even at energies just above the fusion barrier [8,39–41]. These findings have motivated many to investigate ICF at relatively low bombarding energies. However, a clear and robust modeling of ICF processes is still lacking, especially at relatively low bombarding energies, where a clear systematic study is available for a few projectile-target systems. As such, in this work we study the ICF dynamics for energies close to and above the Coulomb barrier of the  $^{12}\text{C} + ^{52}\text{Cr}$  system. Excitation functions (EFs) for various evaporation residues produced in the interaction of the  $^{12}\text{C} + ^{52}\text{Cr}$  system are measured using the thick target-catcher technique at six projectile energies ( $E_{\text{proj}}$ ) up to 87 MeV for reaction products that may be populated via CF and/or ICF processes. It may be pointed out that the charge product ( $Z_1 \cdot Z_2 = 144$ ) for the system is far less than 1600 and, therefore, the probability for possible fission reactions is negligible [42]. Results of the present work may also provide a new cross-section database for several residues produced in the reaction. Further, in this work, an attempt is made to estimate the ICF fraction from production cross sections.

In Sec. II, a brief description of the experimental procedure used in this work is given. Section III presents a comparison of experimental data with values predicted by theoretical models and an interpretation and analysis of the outcome of the comparison. In Sec. IV the ICF fraction is deduced and analyzed before a conclusion is drawn in Sec. V.

## II. EXPERIMENTAL PROCEDURE

The experiment was carried out using the general purpose scattering chamber (GPSC) facility found at the Inter-University Accelerator Center (IUAC), New Delhi, India. A stack containing  $^{52}\text{Cr}$  samples was irradiated by a  $^{12}\text{C}^{6+}$  beam at 87 MeV in the GPSC (the chamber has a facility of in-vacuum transfer of targets, which minimizes the time

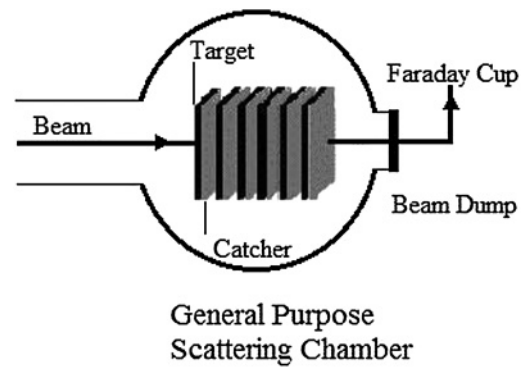


FIG. 1. Typical experimental setup for EFs measurement using the energy degradation technique.

lapse between the stopping of irradiation and the beginning of counting). A typical stacked foil arrangement used for excitation function measurements is shown in Fig. 1. The irradiation of the stack covered the desired energy range of  $\approx 51$ –87 MeV in measuring the EFs of various evaporation residues produced in the  $^{12}\text{C} + ^{52}\text{Cr}$  system. The beam currents were  $\approx 40$  nA throughout the irradiations.  $^{52}\text{Cr}$  targets of thickness  $\approx 364 \pm 4 \mu\text{g}/\text{cm}^2$ , backed by Al catchers of thickness  $2 \text{ mg}/\text{cm}^2$ , were placed after each target normal to the beam direction so that the recoiling nuclei coming out of the target could be trapped in the catcher foil and there would be no loss of activity. To ensure more efficient collection of CF and ICF products, the thickness of Al backings was carefully chosen. The incident flux of the  $^{12}\text{C}$  beam was determined from the charge collected in the Faraday cup (using an ORTEC current integrator device), as well as from the counts of the two Rutherford monitors kept at  $\pm 10^\circ$  to the beam direction. The two sets of values were found to agree with each other, any difference between them being within the 5% range (of the values).

The stack was irradiated for  $\approx 6$  h, keeping in mind the half-lives of interest. The activities induced in the catcher-target assembly were followed off-line, using precalibrated CANBERA's HPGGe detector coupled to CAMAC and based on the FREEDOM data acquisition system developed by the IUAC [43]. The average time between the end of the irradiation and the beginning of the measurements with HPGGe was  $\approx 7$  min. The nuclear spectroscopic data used in the evaluations and measurements of cross sections were taken from the radioactive isotopes data table of Browne and Firestone [44] and are given in Table I.

The spectrometer was calibrated for energy, and efficiency was measured using various standard sources, i.e.,  $^{152}\text{Eu}$ ,  $^{60}\text{Co}$ ,  $^{57}\text{Co}$ , and  $^{133}\text{Ba}$ . Details of geometry-dependent efficiency measurements used in this work are similar to those used by Gupta *et al.* [45]. The residues produced from various reaction channels were identified by their characteristic  $\gamma$  ray and decay curve analysis. The details of the experimental arrangements, formulations, and data reduction procedures used in the present work are similar to those in the work of Agrawal *et al.* [46]. The standard formulation reported in Ref. [46] was used to determine the production cross sections of various reaction products.

TABLE I. Decay characteristics of nuclides studied in the  $^{12}\text{C} + ^{52}\text{Cr}$  system.

Reaction	Nuclide	Half-life	$\gamma$ ray energy (keV)	$I\gamma$ , $\gamma$ /decay (%)
$^{52}\text{Cr}(^{12}\text{C}, 2n)$	$^{62}\text{Zn}$	9.26 h	596.7, 408.3	25.7, 25.2
$^{52}\text{Cr}(^{12}\text{C}, p2n)$	$^{61}\text{Cu}$	3.41 h	282.96, 656.01	12.5, 10.6
$^{52}\text{Cr}(^{12}\text{C}, p3n)$	$^{60}\text{Cu}$	23.2 min	1332.5	88
$^{52}\text{Cr}(^{12}\text{C}, \alpha 3n)$	$^{57}\text{Ni}$	1.5 d	1377.6, 1919.5	77.9, 14.7
$^{52}\text{Cr}(^{12}\text{C}, \alpha 4n)$	$^{56}\text{Ni}$	6.1 d	158.4, 811.9	98.8, 86
$^{52}\text{Cr}(^{12}\text{C}, \alpha pn)$	$^{58}\text{Co}$	70.91 d	810.8	99.5
$^{52}\text{Cr}(^{12}\text{C}, \alpha p2n)$	$^{57}\text{Co}$	271.77 d	122.06	85.5
$^{52}\text{Cr}(^{12}\text{C}, \alpha p3n)$	$^{56}\text{Co}$	77.7 d	846.8	99.9

The various factors that may introduce errors and uncertainties in the present cross-section measurements and their estimates are the following:

- (i) The nonuniform thickness of samples may lead to uncertainty in determining the number of target nuclei. To check the extent of the nonuniformity of the sample, the thickness of each sample was measured at different positions using an  $\alpha$ -transmission method. It is estimated that the error in the thickness of the sample materials is less than 1%.
- (ii) Fluctuation in the beam current may result in variation of the incident flux; proper care was taken to keep the beam current constant as much as possible. The error due to this factor was incorporated by taking the weighted average of the beam current and is estimated to be less than 2%.
- (iii) The dead time in the spectrometer may lead to a loss in the counts. By suitably adjusting the sample-detector distance, the dead time was kept below 10%. These errors exclude uncertainty of the nuclear data, such as branching ratio, decay constant, etc., which have been taken from Ref. [44].
- (iv) Uncertainty in determining the geometry-dependent detector efficiency may also introduce some error, which is estimated to be less than 2%.
- (v) Errors due to a decrease in the carbon ion beam intensity caused by scattering while transferring through the stack are estimated to be less than 1%.

Attempts were made to minimize the uncertainties caused by all the above factors. The overall error in the present work is estimated to be less than or equal to 17%. The experimentally

measured cross sections for the production of various residues in the  $^{12}\text{C} + ^{52}\text{Cr}$  systems via CF and/or ICF processes are given in Table II.

### III. RESULTS AND ANALYSIS

EFs for residues produced in the  $^{12}\text{C} + ^{52}\text{Cr}$  system via CF and/or ICF processes were measured at projectile energies up to 87 MeV. To investigate the ICF reaction dynamics, the EFs for  $^{62}\text{Zn}$ ,  $^{60}\text{Cu}$ ,  $^{61}\text{Cu}$ ,  $^{56}\text{Ni}$ ,  $^{57}\text{Ni}$ ,  $^{56}\text{Co}$ ,  $^{57}\text{Co}$ , and  $^{58}\text{Co}$  radionuclides produced in this energy range were considered. The cross sections from a given reaction channel were determined separately from the observed intensities of all possible identified  $\gamma$  rays, arising from the same radionuclide. The reported values are the weighted average of the various cross-section values obtained [47]. An analysis of experimentally measured EFs was made by comparing them with the theoretical predictions of the statistical model code, PACE4 [48].

In the present work PACE4 rather than ALICE-91 was chosen to predict the EFs of all measurable reaction channels populated in the interaction of the  $^{12}\text{C} + ^{52}\text{Cr}$  system. The PACE4 code uses a Monte Carlo procedure to determine the decay sequence of an excited nucleus using the Hauser-Feshback formalism. This formalism, unlike in the ALICE-91 code, takes angular momentum directly into account. The angular momentum projections are calculated at each stage deexcitation, which enables the determination of the angular distribution of emitted particles. The main advantage of PACE4 calculations over ALICE-91 calculations is that they provide correlations between various quantities, such as particles and  $\gamma$

TABLE II. Cross sections in mb for residues in the  $^{12}\text{C} + ^{52}\text{Cr}$  system measured experimentally. The sum of the measured evaporation residue (ER) cross sections,  $\sum\sigma_{\text{ER}}$ , and the percentage of the cross section covered by the measured ER,  $\% \sum\sigma_{\text{ER}}$ , the total cross section, is based on PACE4 calculations.

$E_{\text{proj}}$ (MeV)	$^{62}\text{Zn}$	$^{60}\text{Cu}$	$^{61}\text{Cu}$	$^{56}\text{Ni}$	$^{57}\text{Ni}$	$^{58}\text{Co}$	$^{57}\text{Co}$	$^{56}\text{Co}$	$\sum\sigma_{\text{ER}}$	$\% \sum\sigma_{\text{ER}}$
$51.5 \pm 1.1$	$11.8 \pm 2.0$	$4.1 \pm 0.7$	$208.5 \pm 35.4$	–	$27.1 \pm 4.6$	$317.9 \pm 54.0$	$97.8 \pm 16.6$	–	$667.2 \pm 66.9$	45.4
$60.0 \pm 0.9$	$6.9 \pm 1.2$	$225.2 \pm 4.3$	$142 \pm 24.1$	–	$79.5 \pm 13.5$	$278.8 \pm 47.4$	$343.4 \pm 58.4$	–	$875.8 \pm 80.3$	46.6
$67.3 \pm 1.6$	–	$57.8 \pm 9.8$	$91.2 \pm 15.5$	–	$113.8 \pm 19.4$	$165.8 \pm 28.2$	$598.8 \pm 101.8$	$86.5 \pm 14.7$	$1113.9 \pm 109.9$	49.2
$74.1 \pm 1.0$	–	$53.7 \pm 9.1$	$72.8 \pm 12.4$	$26.9 \pm 4.6$	$128.3 \pm 21.8$	$87.8 \pm 14.9$	$637.0 \pm 108.3$	$208.3 \pm 35.4$	$1214.8 \pm 118.1$	48.2
$79.5 \pm 0.9$	–	$41.3 \pm 7.0$	$220.8 \pm 37.5$	$44.4 \pm 7.5$	$131.7 \pm 22.4$	$69.9 \pm 11.8$	$534.3 \pm 90.8$	$473.5 \pm 80.5$	$1515.9 \pm 129.9$	44.4
$86.4 \pm 1.5$	–	$23.4 \pm 4.0$	$97.9 \pm 16.6$	$55.5 \pm 9.4$	$104.5 \pm 17.8$	$112.8 \pm 19.3$	$378.7 \pm 64.4$	$687.4 \pm 116.8$	$1460.2 \pm 137.3$	38.6

TABLE III. Columns with beam energy, Bass fusion cross section, Bass fusion barrier and radius, Yrast spin at maximum excitation energy,  $L$  diffuseness,  $L$  at grazing, and fission barrier.

$E_{\text{proj}}$ (MeV)	Bass fusion cross-section	Fusion radius, fusion barrier	Yrast spin	Diffuseness ( $\Delta$ )	$l_{\text{max}}$	Fission barrier
$51.5 \pm 1.1$	1112 mb	7.90 fm, 21.08 MeV	$39 \hbar$	$4 \hbar$	$\approx 25 \hbar$	49.63 MeV
$60.0 \pm 0.9$	1203 mb	6.05 fm, 21.08 MeV	$42 \hbar$	$4 \hbar$	$\approx 28 \hbar$	49.63 MeV
$67.3 \pm 1.6$	1197 mb	6.05 fm, 21.08 MeV	$44 \hbar$	$4 \hbar$	$\approx 30 \hbar$	49.63 MeV
$74.1 \pm 1.0$	1193 mb	6.05 fm, 21.08 MeV	$46 \hbar$	$4 \hbar$	$\approx 31 \hbar$	49.63 MeV
$79.5 \pm 0.9$	1190 mb	6.05 fm, 21.08 MeV	$47 \hbar$	$4 \hbar$	$\approx 32 \hbar$	49.63 MeV
$86.4 \pm 1.5$	1187 mb	6.05 fm, 21.08 MeV	$49 \hbar$	$4 \hbar$	$\approx 34 \hbar$	49.63 MeV

rays or angular distribution of particles. The code also provides the ability to have an event-by-event trace back of the entire decay sequence from the CN system into any one of the exit channels.

The process of deexcitation of the excited nuclei was calculated using the PACE4 statistical model code which follows the correct procedure for angular momentum coupling at each stage of deexcitation. The angular momentum conservation is explicitly taken into account at each step. For any specific bombarding energy, the partial cross section for CN formation at angular momentum  $l$ ,  $\sigma_l$ , is

$$\sigma_l = \frac{\lambda^2}{4\pi} (2l + 1) T_l, \quad (1)$$

where  $\lambda$  is the reduced wave length and  $T_l$ , the transmission coefficient, is given by the expression

$$T_l = \left[ 1 + \exp\left(\frac{l - l_{\text{max}}}{\Delta}\right) \right]^{-1}, \quad (2)$$

where  $\Delta$  is a diffuseness parameter and  $l_{\text{max}}$ , the maximum amount of  $l$  detained by total fusion cross section, is determined by

$$\sigma_F = \sum \sigma_l. \quad (3)$$

The transmission coefficients for the emission of light particles ( $n$ ,  $p$ , and  $\alpha$ ) during the deexcitation were determined using optical model calculations [49–51]. In this calculation the input fusion cross section was calculated using the Bass formula [52]. (The values of Bass fusion cross sections used in the present work are given in Table III.) The evaporation residue cross section was then determined by two other parameters: (1) the ratio of level densities at the saddle point and at the ground state and (2) the height of the fission barrier (which depends on the total spin). In these calculations, the deexcitation process, which used 100 000 de-excitation cascades, was followed by a Monte Carlo procedure. The statistical errors in the maxima of the EFs (for all ER considered in the present work) were less than 5%. Transmission coefficients for the evaporation of light particles ( $n$ ,  $p$ , and  $\alpha$ ) were obtained during the first step of deexcitation by a full optical model calculation. Angular momentum projections were calculated at each stage of deexcitation, enabling the determination of the angular distribution of the emitted particles. Three parameters were involved in determining the various level densities needed for the calculations: the “little  $a$ ” parameter involved in

particle evaporation calculation, the ratio  $a_f/a$  of the little  $a$  parameter at the saddle point and ground state deformations, and  $B_f$ —the fission barrier, which is taken to be equal to the rotating liquid drop fission barrier. In the description of  $\gamma$ -ray competitions, emission of  $E1$ ,  $M1$ ,  $E2$ , and  $M2$   $\gamma$  rays and  $\gamma$  ray strength for different transitions are taken from the systematic default values. The  $\gamma$ -decay intensities in Weisskopf units were 0.00008, 0.025, 4.8, and 0.0195 for  $E1$ ,  $M1$ ,  $E2$ , and  $M2$ , respectively. In this code the level density parameter  $a$ , which largely affects the equilibrium state components of a cross section is calculated from the expression  $a = A/K \text{ MeV}^{-1}$ , where  $A$  is the nucleon number of a compound system and  $K$  is an adjustable constant, which may be varied to match the experimental data. The experimentally measured EFs were compared with PACE4 predictions using different level density parameter values for the evaporation residues produced via the CF reaction. For the evaporation residues  $^{60}\text{Cu}$ ,  $^{61}\text{Cu}$ , and  $^{62}\text{Zn}$ , the value of  $K$  was varied ( $K =$  values of 8, 10, 12, 14, and 15 were used) to match the experimental data and the results are displayed in Figs. 2(a)–2(c). In Table III the most important input parameters used to perform the PACE4 calculations are listed.

#### A. ( $^{12}\text{C}$ , $xn$ ) and ( $^{12}\text{C}$ , $pxn$ ) channels

The measured EFs along with theoretical predictions obtained from PACE4 for possible residues populated via ( $^{12}\text{C}$ ,  $2n$ ) and ( $^{12}\text{C}$ ,  $pxn$ ) ( $x = 2, 3$ ) channels are shown in Figs. 2(a)–2(c). Obviously in these sets of channels, there is no likelihood of ICF reactions, and therefore, these sets of channels are populated only by CF. Note that in the case of ( $^{12}\text{C}$ ,  $pxn$ ) channels, the residue  $^{61}\text{Cu}$  via the ( $^{12}\text{C}$ ,  $p2n$ ) channel may be formed directly through the reaction  $^{12}\text{C} + ^{52}\text{Cr} \rightarrow ^{61}\text{Cu} + p2n$ .

It may also be populated by electron capture (EC)/ $\beta^+$ -emission of the higher charge isobar precursor (HCIP) residual nucleus  $^{61}\text{Zn}$ , formed through the reaction  $^{12}\text{C} + ^{52}\text{Cr} [^{64}\text{Zn}]^* \rightarrow [^{61}\text{Zn}]^* + 3n [^{61}\text{Zn}]^* \rightarrow ^{61}\text{Cu} + \text{EC}/\beta^+$ .

Since the precursor  $^{61}\text{Zn}$  has a relatively shorter half-life of 1.48 min compared to the 3.408 h half-life of the daughter nucleus  $^{61}\text{Cu}$ , the measured activity of the residue  $^{61}\text{Cu}$  has a contribution from the precursor.

An attempt was made to separate out the contribution due to precursor decay from the cumulative activity of  $^{61}\text{Cu}$ . The cumulative (cum) cross section,  $\sigma_{\text{cum}}$ , of a given residue is the sum of (i) its independent (ind) production cross section,  $\sigma_{\text{ind}}$ ,

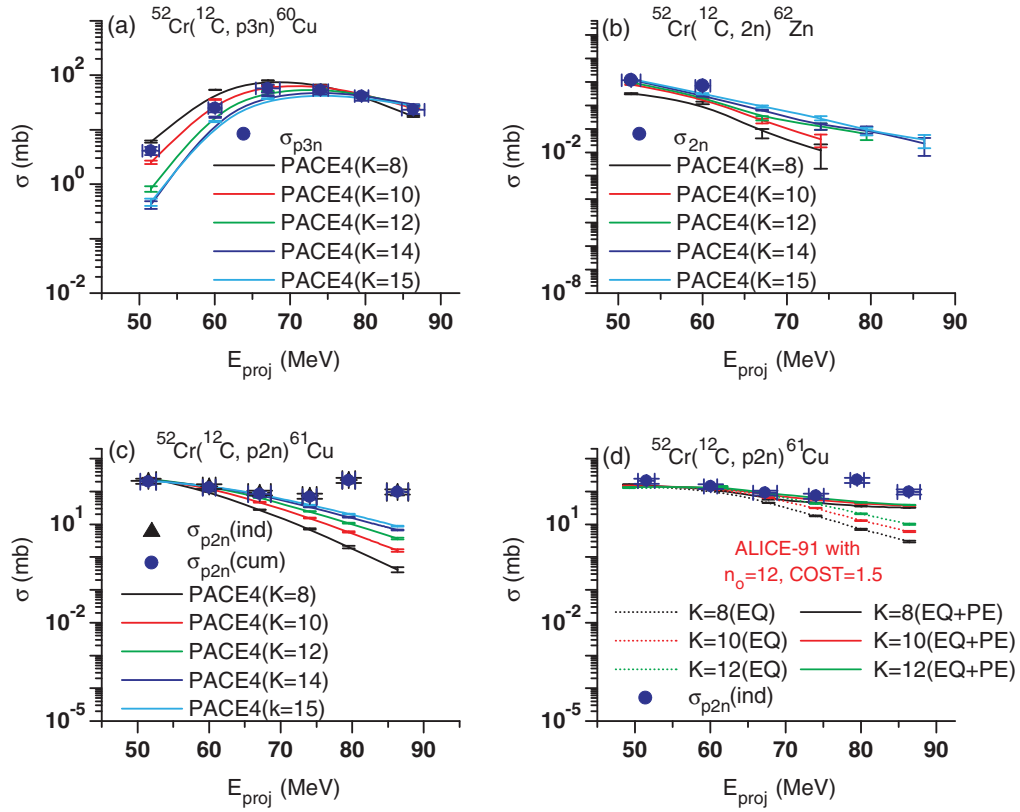


FIG. 2. (Color online) Experimentally measured and theoretically calculated EFs for different residues via  $(^{12}\text{C}, 2n)$  and  $(^{12}\text{C}, pxn)$  channels in the  $^{12}\text{C} + ^{52}\text{Cr}$  system at  $\approx 51\text{--}87$  MeV. The curves in panels (a)–(c) represent the theoretical predictions of the PACE4 statistical model code at different values of  $K$  ( $K = 8, 10, 12, 14,$  and  $15$ ), and the solid and broken curves in panel (d), respectively, represent the prediction of ALICE-91 with and without incorporating the contribution of PE emission at different values of  $K$  ( $K = 8, 10,$  and  $12$ ),  $n_0 = 12$ , and  $\text{COST} = 1.5$ . The solid circles represent the measured cross sections; solid triangles represent the deduced independent cross sections (if any).

deduced from the measured cumulative cross section using the relationship in Eq (4), and (ii) the cross section for independent production of its precursor,  $\sigma_{\text{prec}}$ , multiplied by a numerical coefficient,  $F_{\text{prec}}$  [2],

$$\sigma_{\text{cum}} = \sigma_{\text{ind}} + F_{\text{prec}}\sigma_{\text{prec}}. \quad (4)$$

The value of  $F_{\text{prec}}$  depends on the branching ratio  $B_{\text{prec}}$  for precursor decay to the residue and is given by

$$F_{\text{prec}} = B_{\text{prec}} \frac{T_{\text{ind}}}{T_{\text{ind}} - T_{\text{prec}}}, \quad (5)$$

where  $T_{\text{ind}}$  and  $T_{\text{prec}}$  are the half-lives of the residue and the precursor, respectively. As such, the cumulative cross section is given by

$$\sigma_{\text{cum}} = \sigma_{\text{ind}} + B_{\text{prec}} \frac{T_{\text{ind}}}{T_{\text{ind}} - T_{\text{prec}}} \sigma_{\text{prec}}. \quad (6)$$

The values of branching ratios and half-lives required for obtaining the  $B_{\text{prec}}$  coefficients are taken from the tables of the Nuclear Wallet Cards [53]. Using the above formulation in the present case, the cumulative measured yield,  $\sigma_{\text{cum}}^{\text{meas}}(^{61}\text{Cu})$ , and the deduced independent yield,  $\sigma_{\text{ind}}(^{61}\text{Cu})$ , for  $^{61}\text{Cu}$  are related by the equation

$$\sigma_{\text{cum}}^{\text{meas}}(^{61}\text{Cu}) = \sigma_{\text{ind}}(^{61}\text{Cu}) + 1.0073\sigma_{\text{prec}}^{\text{PACE4}}(^{61}\text{Zn}). \quad (7)$$

Here,  $\sigma_{\text{prec}}^{\text{PACE4}}(^{61}\text{Zn})$  is the independent yield of its precursor, estimated using the PACE4 code.

As such, the precursor contribution of  $^{61}\text{Cu}$  at different energies was subtracted from the cumulative yield to separate out the independent yield. The measured cumulative cross sections,  $\sigma_{\text{cum}}^{\text{meas}}(^{61}\text{Cu})$ , as well as the deduced independent cross sections,  $\sigma_{\text{ind}}(^{61}\text{Cu})$ , for the  $^{61}\text{Cu}$  residue deduced in this way are plotted in Fig. 2(c). It may be seen from this figure that the contribution of the precursor,  $^{61}\text{Zn}$ , to the production of  $^{61}\text{Cu}$  is relatively small. As can be seen from Figs. 2(a)–2(c) the theoretically calculated EFs corresponding to the level density parameter  $K = 10$  in general reproduced satisfactorily experimentally measured EFs for the residues  $^{62}\text{Zn}$ ,  $^{61}\text{Cu}$ , and  $^{60}\text{Cu}$  produced in the CF processes of the  $^{12}\text{C}$  projectile with the target  $^{52}\text{Cr}$ . However, in Fig. 2(c), at the tail section of the excitation function, the measured cross sections were higher than the values predicted by PACE4. This higher measured cross section at higher energies may indicate PE emission, which is not taken into account in PACE4 calculations. When  $^{12}\text{C}$  collides with  $^{52}\text{Cr}$ , the orderly translational motion of the nucleons of the projectile and the target transforms gradually into chaotic thermal motion mainly through a sequence of two-body interactions. This thermalization process ends when the composite system reaches a state of thermal equilibrium. During the thermalization

process it may happen that a single nucleon, or clusters of nucleons, which still possess considerable amounts of energy are ejected into the continuum (PE emission). The PE emission leads naturally to an increase in the width of the excitation function since it reduces quite considerably the CN excitation energy and the number of particles that are subsequently evaporated [2].

An attempt was made to confirm contributions of PE emission at higher energy points of the ( $^{12}\text{C}$ ,  $p2n$ ) channel using the ALICE-91 code [54]. The ALICE-91 code, developed by Blann [54], may be used to calculate equilibrium (EQ) as well as PE emission cross sections in light- and heavy-ion-induced reactions. A detailed discussion of this code and the procedures used to set the best combinations of input parameters is given in one of our recent works [46]. However, for the sake of completeness, it must be pointed out that nuclear level density plays a central role in any statistical analysis of nuclear reactions. In this code the most sensitive parameter,  $a$  ( $a = A/K$ , where  $a$ ,  $A$ , and  $K$  are the same as in PACE4), which mainly governs the EQ state, the nucleon-nucleon mean free path multiplier, COST, and initial exciton number,  $n_o$  (which represents the initial configuration of the composite system) are some of the important parameters.  $K$  largely affects the EQ component, while  $n_o$  and COST govern the PE component. Blann [14] in his study on the role of precompound decay in heavy-ion reactions has indicated that the significant contribution to PE emission may come from the multiple precompound emissions at higher energies and also from equilibration emissions if they take place in the low-density region. He has also pointed out that in heavy-ion reactions all partial waves do not contribute to the fusion, and the spherical shape for the corresponding moment of inertia may not be appropriate. The EFs for the production of  $^{61}\text{Cu}$  calculated using the ALICE-91 code (for  $K$  values of 8, 10, and 12) with/without including the contribution from PE emissions are shown in Fig. 2(d). As can be seen from this figure, the predictions of ALICE-91, after incorporating the contribution from PE emissions, are in considerably better agreement with the measured data at 79.5 and 86.4 MeV than the PACE4 predictions. It may be further observed from Fig. 2(d) that the predicted EF values for different values of  $K$  are mostly similar and, if they differ, the differences are very small.

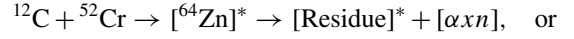
The fact that the measured fusion cross sections for non- $\alpha$ -emitting channels could be reproduced satisfactorily by PACE4 predictions gives confidence in the input parameters chosen to fit the EFs of  $\alpha$ -emitting channels. It may also be observed from Figs. 2(a)–2(c) that the theoretical values obtained using different higher values of level density parameters, where  $K \geq 10$  are mostly similar, and if and when they differ, the differences are very small. In the present work all calculations and analyses were performed consistently using the same set of parameters,  $K = 10$ , for all channels.

### B. ( $^{12}\text{C}$ , $\alpha xn$ ) channels

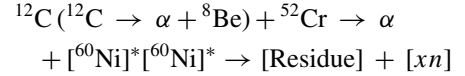
Figures 3(a) and 3(b) display the measured EFs along with the PACE4 predictions for the population of  $^{60-x}\text{Ni}$  ( $x = 3, 4$ )

isotopes via ( $^{12}\text{C}$ ,  $\alpha xn$ ) channels. Note that, in this case, the residues may be formed following two different processes:

(i) by CF of the  $^{12}\text{C}$  with the target followed by the formation of an excited composite nucleus from which evaporation of neutrons and  $\alpha$  particles takes place, i.e.,



(ii) the  $^{12}\text{C}$  ion breaks up into  $\alpha + ^8\text{Be}$  and the  $^8\text{Be}$  projectile fuses with the target leaving an  $\alpha$  particle as a spectator. In this case, the excited nucleus formed by the fusion with  $^8\text{Be}$  may emit  $xn$  particles while deexciting, i.e.,

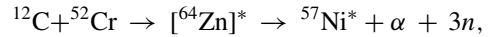


In this work reactions like (i) refer to CF and (ii) to ICF. These modes of reactions may be represented by the following compact equations:

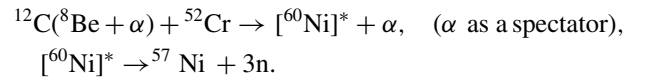


The residue  $^{57}\text{Ni}$  may be populated through CF and/or ICF reactions as

(i) CF of  $^{12}\text{C}$ , i.e.,

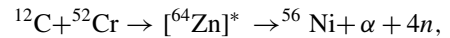


(ii) ICF of  $^{12}\text{C}$ , i.e.,

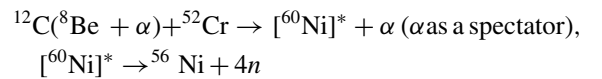


Similarly, the residue,  $^{56}\text{Ni}$ , may be populated through CF and/or ICF channels as

(i) CF of  $^{12}\text{C}$ , i.e.,



(ii) ICF of  $^{12}\text{C}$ , i.e.,



As can be seen from Figs. 3(a) and 3(b), the experimentally measured EFs are relatively higher than the theoretical predictions. Because PACE4 doesn't take ICF into account, therefore the enhancement in the experimentally measured production cross sections may be attributed to the contribution coming from the ICF of  $^{12}\text{C}$  with the target nucleus.

### C. ( $^{12}\text{C}$ , $\alpha pxn$ ) channels

In the case of residues via ( $^{12}\text{C}$ ,  $\alpha pxn$ ) ( $x = 1, 2$ , and 3) channels, there is a likelihood of ICF reactions occurring and, therefore, the residues in these channels may be populated by CF and/or ICF processes.

In Figs. 3(c), 3(d), and 4(a), the measured EFs for  $^{59-x}\text{Co}$  residues formed via ( $^{12}\text{C}$ ,  $\alpha pxn$ ) channels are displayed, together with the PACE4 predicted EFs. Note also that like the residues via ( $^{12}\text{C}$ ,  $\alpha xn$ ) channels, residues via ( $^{12}\text{C}$ ,  $\alpha pxn$ ) channels may also be formed by CF and/or ICF processes as the following.

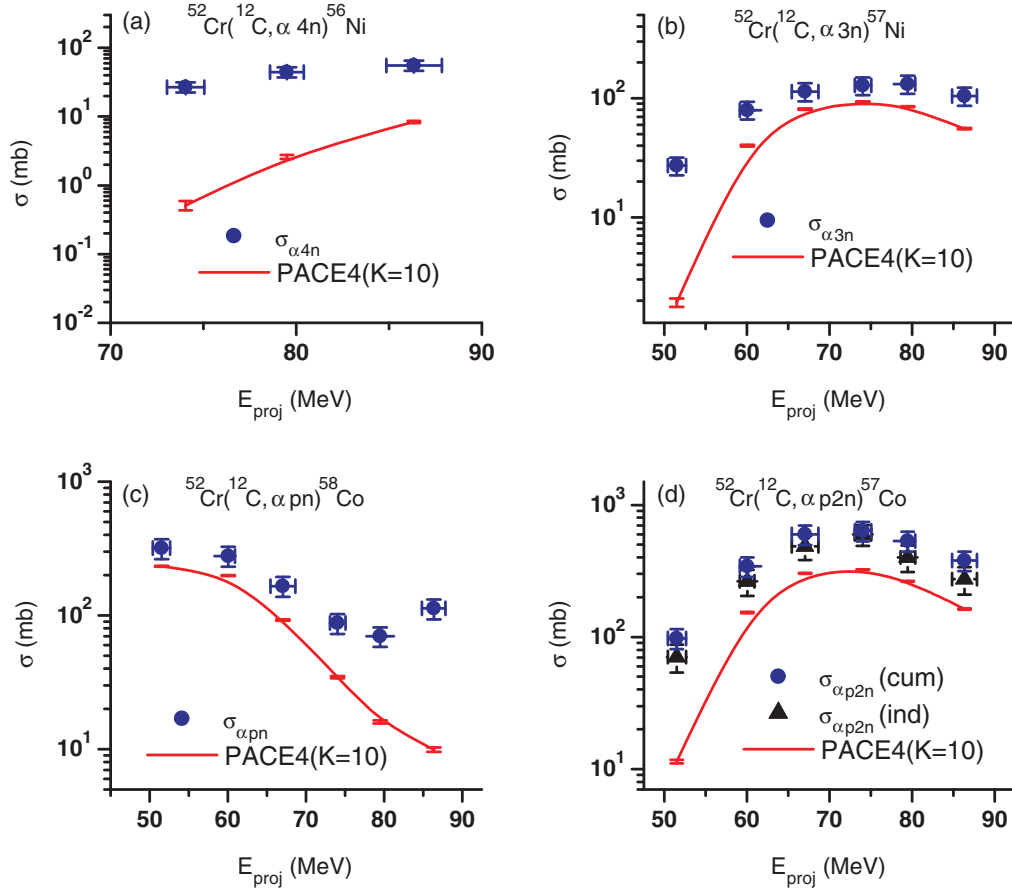
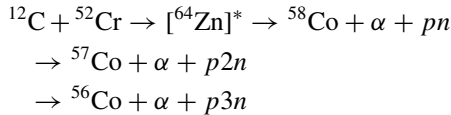
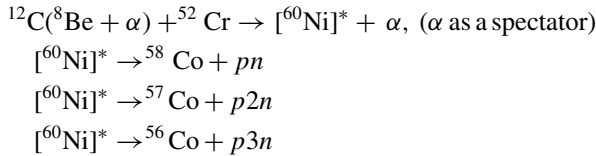


FIG. 3. (Color online) In panels (a)–(d) EFs of the evaporation residues produced via  $(^{12}\text{C}, \alpha xn)$  and  $(^{12}\text{C}, \alpha pxn)$  channels in the  $^{12}\text{C} + ^{52}\text{Cr}$  system at  $\approx 51$ – $87$  MeV are displayed. The solid circles represent the measured cross sections; solid triangles represent the deduced independent cross sections (if any). The curves represent the PACE4 predictions at  $K = 10$ .

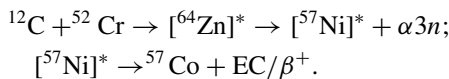
(i) CF of  $^{12}\text{C}$ , i.e.,



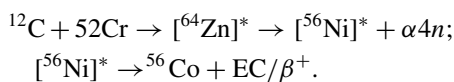
(ii) ICF of  $^{12}\text{C}$ , i.e.,



Further note that in the case of  $(^{12}\text{C}, \alpha pxn)$  channels the residues  $^{57}\text{Co}$  and  $^{56}\text{Co}$  may also be populated by the decay of the HCIP as shown below:



Similarly, the population of residue  $^{56}\text{Co}$  may also be formed by a precursor decay of the type



Using the general formulations discussed before to separate out the independent cross sections from the cumulative one, the two cross sections in  $^{56}\text{Co}$  and  $^{57}\text{Co}$  residues are related by the following equations:

$$\sigma_{\text{cum}}^{\text{meas}}(^{56}\text{Co}) = \sigma_{\text{ind}}(^{56}\text{Co}) + 1.085\sigma_{\text{prec}}^{\text{meas}}(^{56}\text{Ni}), \quad (8)$$

$$\sigma_{\text{cum}}^{\text{meas}}(^{57}\text{Co}) = \sigma_{\text{ind}}(^{57}\text{Co}) + 1.006\sigma_{\text{prec}}^{\text{meas}}(^{57}\text{Ni}). \quad (9)$$

The measured cumulative cross sections,  $\sigma_{\text{cum}}^{\text{meas}}$ , as well as independent cross sections,  $\sigma_{\text{ind}}$ , for  $^{56}\text{Co}$  and  $^{57}\text{Co}$  residues deduced in this way are also plotted in Figs. 3(d) and 4(a). As can be seen from these figures, the contribution of precursors  $^{56}\text{Ni}$  and  $^{57}\text{Ni}$  to the production of  $^{56}\text{Co}$  and  $^{57}\text{Co}$  are relatively small.

It may, however, be pointed out that the cumulative and independent yields of  $^{56}\text{Co}$  and  $^{57}\text{Co}$  reaction products are almost the same in the entire energy range of the  $^{12}\text{C} + ^{52}\text{Cr}$  system.

Further, in Figs. 3 and 4(a) the observed enhancement in the HCIP-decay-subtracted measured cross sections (if any) over theoretical predictions may again be attributed to the fact that these residues are also produced via ICF of the projectile  $^{12}\text{C}$ . It has already been mentioned that all the  $\alpha$ -emitting channels identified in the present work are expected to have significant contributions from ICF processes.

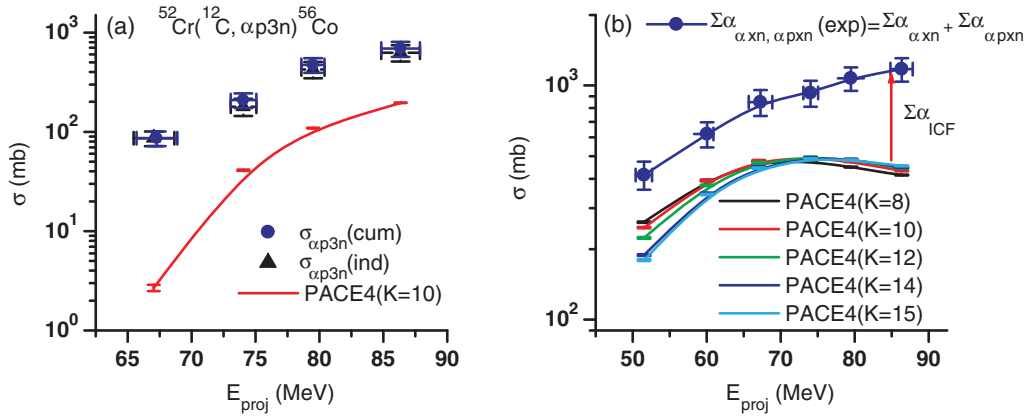


FIG. 4. (Color online) Panel (a) shows the measured cumulative and the deduced independent cross sections for the ( $^{12}\text{C}$ ,  $\alpha p3n$ ) channel, and panel (b) shows a comparison of the total sum of the HCIP-decay-subtracted measured cross sections,  $\Sigma\sigma_{\alpha xn, \alpha pxn}(\text{exp}) = \Sigma\sigma_{\alpha xn} + \Sigma\sigma_{\alpha pxn}$  and the total sum of the calculated cross sections using PACE4,  $\Sigma\sigma_{\alpha xn, \alpha pxn}(\text{theo})$ , at different values of  $K$  ( $K = 8, 10, 12, 14$ , and  $15$ ). The curves connecting the experimental data points in panel (b) are just to guide the eyes.

To determine the contributions of ICF processes in the ( $^{12}\text{C}$ ,  $\alpha xn$ ) and ( $^{12}\text{C}$ ,  $\alpha pxn$ ) channels, the sum of the measured cross sections  $\Sigma\sigma_{\alpha xn, \alpha pxn}(\text{exp}) = \Sigma\sigma_{\alpha xn}(\text{exp}) + \Sigma\sigma_{\alpha pxn}(\text{exp})$  was compared with the corresponding values calculated using the statistical model code PACE4, i.e.,  $\Sigma\sigma_{\alpha xn, \alpha pxn}(\text{theo}) = \Sigma\sigma_{\alpha xn}(\text{theo}) + \Sigma\sigma_{\alpha pxn}(\text{theo})$ . Because the code does not take ICF in to account, the difference between these two values represents the ICF contribution.

In Fig. 4(b) a comparison of the sum of HCIP-decay-subtracted measured cross sections,  $\Sigma\sigma_{\alpha xn, \alpha pxn}(\text{exp}) = \Sigma\sigma_{\alpha xn}(\text{exp}) + \Sigma\sigma_{\alpha pxn}(\text{exp})$ , was made with the sum of the calculated cross sections,  $\Sigma\sigma_{\alpha xn, \alpha pxn}(\text{theo}) = \Sigma\sigma_{\alpha xn}(\text{theo}) + \Sigma\sigma_{\alpha pxn}(\text{theo})$ , for different values of physically acceptable level density parameters, i.e.,  $K = 8, 10, 12, 14$ , and  $15$ . As can be seen from this figure, the calculated sum,  $\Sigma\sigma_{\alpha xn, \alpha pxn}(\text{theo})$ , did not reproduce the measured one,  $\Sigma\sigma_{\alpha xn, \alpha pxn}(\text{exp})$ , in the entire energy range, though the patterns of the two sets of sums showed a strong correlation.

Further, the difference between  $\Sigma\sigma_{\alpha xn, \alpha pxn}(\text{exp})$  and  $\Sigma\sigma_{\alpha xn, \alpha pxn}(\text{theo})$ , which is shown as  $\Sigma\sigma_{\text{ICF}}$  for  $K = 10$ , was found to increase with beam energy, indicating the increased

significance of ICF processes at relatively higher energy values.

Here  $\Sigma\sigma_{\text{ICF}}$  was assigned to the difference between the sum of HCIP-decay-subtracted measured cross sections,  $\Sigma\sigma_{\alpha xn, \alpha pxn}(\text{exp})$ , and the sum of the calculated cross-sections,  $\Sigma\sigma_{\alpha xn, \alpha pxn}(\text{theo})$ , at  $K = 10$  and was plotted as a function of projectile energy. It is clearly seen from Fig. 5(a) that ICF production cross sections  $\Sigma\sigma_{\text{ICF}}$  increase significantly with increases in beam energy.

In Fig. 5(b), the HCIP-decay-subtracted total CF cross sections,  $\Sigma\sigma_{\text{CF}} [\Sigma\sigma_{\text{CF}} = \sigma_{2n}(\text{exp}) + \Sigma\sigma_{pxn}(\text{exp}) + \Sigma\sigma_{\alpha xn}(\text{theo}) + \Sigma\sigma_{\alpha pxn}(\text{theo})]$ , and total measured cross sections,  $\sigma_{\text{TF}} (\sigma_{\text{TF}} = \Sigma\sigma_{\text{CF}} + \Sigma\sigma_{\text{ICF}})$ , for all (measurable) reaction channels in the  $^{12}\text{C} + ^{52}\text{Cr}$  system are compared. As can be seen from this figure, with the increase in energy the difference between  $\sigma_{\text{TF}}$  and  $\Sigma\sigma_{\text{CF}}$  continues to increase, indicating the dominance of ICF processes at relatively higher energies. This may be due to an increase in the probability of the fragmentation of a projectile into  $\alpha$  clusters [ $^8\text{Be} (\alpha + \alpha) + \alpha$ ] as the projectile energy increases.

For projectile energy above the Coulomb barrier ( $V_{\text{CB}}$ ), where  $E_{\text{c.m.}} > V_{\text{CB}}$ , the capture cross section for charged

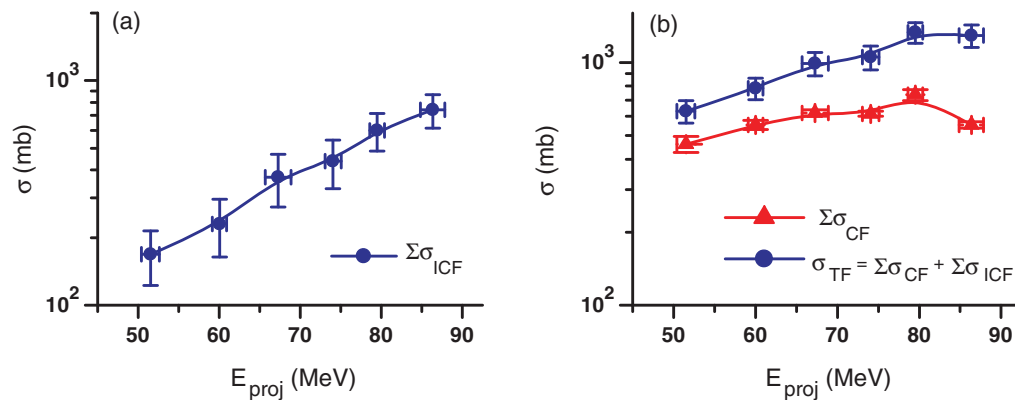


FIG. 5. (Color online) In panel (a) the total sum of ICF cross sections,  $\Sigma\sigma_{\text{ICF}}$ , for ( $^{12}\text{C}$ ,  $\alpha xn$ ) and ( $^{12}\text{C}$ ,  $\alpha pxn$ ) channels and in panel (b) a comparison of the total sum of all possible measured cross sections  $\sigma_{\text{TF}}$  and the total sum of CF cross sections  $\Sigma\sigma_{\text{CF}}$  are shown. The curves connecting the data points are just to guide the eyes.

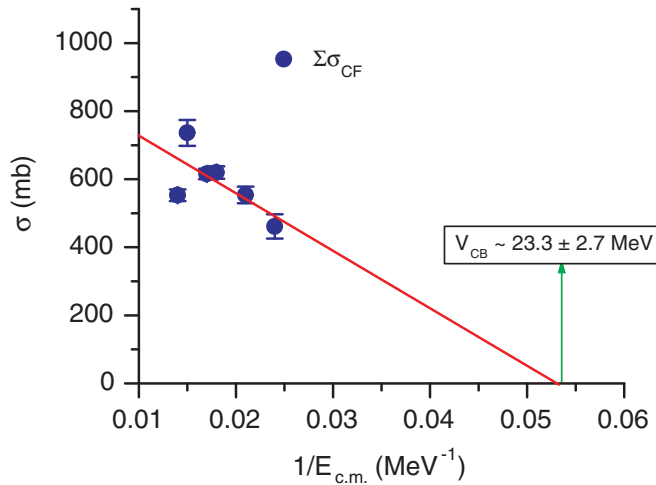


FIG. 6. (Color online) CF cross sections as the function  $1/E_{c.m.}$  for the  $^{12}\text{C} + ^{52}\text{Cr}$  system found to reproduce the  $V_{CB}$  of the present work within the range of the experimental error.

particles by a nucleus in the classical picture of a Weisskopf formulation [55] is given by

$$\sigma_{CF} = \pi R_o^2 \left(1 - \frac{V_{CB}}{E_{c.m.}}\right), \quad (10)$$

where  $E_{c.m.}$  is the energy in a center-of-mass system. As such, if  $\Sigma\sigma_{CF}$  is plotted against  $1/E_{c.m.}$ , it should reproduce a linear curve.

The HCIP-decay-subtracted fusion cross-section values,  $\Sigma\sigma_{CF}$ , were plotted as a function of  $1/E_{c.m.}$  in Fig. 6. A fit to the  $\Sigma\sigma_{CF}$  data points indicates a linear curve that cuts the  $x$  axis at the beam energy equal to  $V_{CB}$  within the range of the error bar. The reproduction of the interaction barrier ( $\approx V_{CB}$ ) allows us to extract the corresponding interaction radius ( $R_o \approx R_{fus}$ ), the maximum distance at which fusion can take place for  $l = 0$ . Values of  $R_o$  (here,  $R_o \approx 15.1 \pm 3.7$  fm) that were obtained in this way turned out to be significantly larger than the interaction for two touching spherical nuclei in the liquid drop model [56]. Thus, only certain nuclear densities overlap at the interaction radius. These results may also indicate that the nuclear shape is distorted with increasing angular momentum until a critical angular momentum is reached for which the nuclear shape is no longer stable. Thus, above this critical angular momentum, CF will not occur.

Further, it may be pointed out that the observed departure from linearity substantially above  $V_{CB}$  may indicate the approach to and the beginning of a quantal region giving rise to sub-barrier fusion.

#### IV. INCOMPLETE FUSION FRACTION

To investigate the energy dependence of the ICF contribution to energy for the  $^{12}\text{C} + ^{52}\text{Cr}$  system, the percentage fraction of the ICF process ( $P_{ICF} = \sum \sigma_{ICF}/\sigma_{TF} \cdot 100\%$ ) was deduced. Figure 7 represents the graph of  $P_{ICF}$  as a function of normalized projectile energy ( $E_{Proj}/V_{CB}$ ), for the presently studied system, along with several other systems available in the literature [8,19–21,45]. As can be seen from this figure,

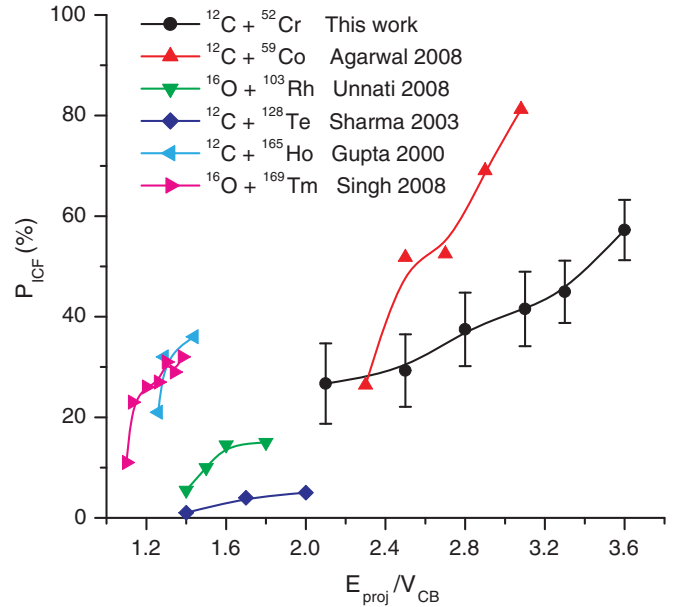


FIG. 7. (Color online) The percentage ICF fraction as a function of normalized projectile energy for the  $^{12}\text{C} + ^{52}\text{Cr}$  system along with values of systems available in the literature (Agarwal 2008 [46], Unnati 2008 [19], Sharma 2003 [21], Gupta 2000 [20], and Singh 2008 [8]). The curves connecting the data points are to direct the eyes.

$P_{ICF}$  increases with the increase in normalized projectile energy for all the systems.

Moreover, to study the dependence of  $P_{ICF}$  on entrance channel mass asymmetry, a pair of  $P_{ICF}$  are plotted in Fig. 8 as a function of normalized relative velocity,  $v_{rel}/c$ ,

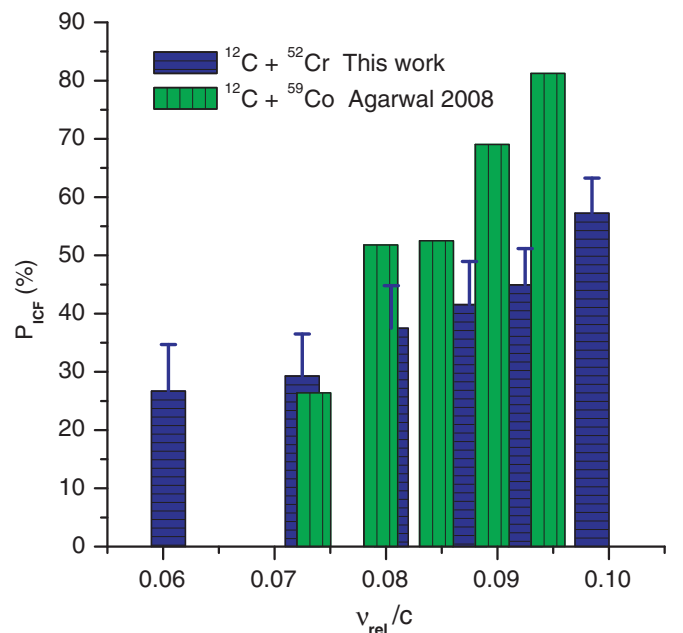


FIG. 8. (Color online) The percentage ICF fraction as a function of normalized velocity,  $v_{rel}/c$ , in the  $^{12}\text{C} + ^{52}\text{Cr}$  and  $^{12}\text{C} + ^{59}\text{Co}$  (Agarwal 2008 [46]) systems.

for  $^{12}\text{C} + ^{52}\text{Cr}$  and  $^{12}\text{C} + ^{59}\text{Co}$  systems where

$$v_{\text{rel}} = \left[ \frac{2(E_{\text{c.m.}} - V_{\text{CB}})}{\mu} \right]^{\frac{1}{2}}, \quad (11)$$

$\mu$  is the reduced mass of the system and  $E_{\text{c.m.}}$  is the center-of-mass energy. The data are plotted against  $v_{\text{rel}}/c$ , which takes into account the difference in  $V_{\text{CB}}$  between the two systems. It is found that the value of  $P_{\text{ICF}}$  in the  $^{12}\text{C} + ^{52}\text{Cr}$  system is higher than that observed for a  $^{12}\text{C} + ^{59}\text{Co}$  system for the measured energy range. The difference between the two systems may indicate the impact of  $P_{\text{ICF}}$  on entrance channel mass asymmetry ( $\frac{A_T}{A_T + A_P}$ ). Further, the data suggest that the probability of ICF is more in a mass-asymmetric system than in a symmetric system, which is consistent with the systematic presented by Morgenstern *et al.* [57].

## V. CONCLUSION

We measured the EFs of eight evaporation residues formed in the  $^{12}\text{C} + ^{52}\text{Cr}$  reaction at several beam energies ranging from  $\approx 51$  to 87 MeV. The experimental data were compared with the values obtained using the PACE4 statistical model code. The measured CF cross sections revealed an agreement with the PACE4 values, especially in the lower energy region. For a ( $^{12}\text{C}, p2n$ ) channel the measured excitation functions at the tail sections were better reproduced by calculations made using the ALICE-91 code, which takes into account contributions from PE emissions. This result is further proof of the importance of

a proper admixture of EQ and PE processes in the prediction of EFs.

For  $\alpha$ -emitting channels, the measured cross sections were significantly higher than the values predicted by PACE4. This enhancement in the measured cross sections is attributable to the prompt break-up of the projectile into  $\alpha$  clusters wherein the projectile,  $^{12}\text{C}$ , breaks up into  $^8\text{Be} + ^4\text{He}$ , leading to an ICF reaction.

From an analysis of the relative yields of ICF products, we conclude that in addition to CF, ICF is a process of great importance even at these lower energies. Thus, it is important when predicting total reaction cross sections to take into account the ICF contributions.

Further, as expected, in the reaction of  $^{12}\text{C}$  and  $^{52}\text{Cr}$ , the sum of ICF cross sections,  $\Sigma\sigma_{\text{ICF}}$ , was found to increase with energy.

## ACKNOWLEDGMENTS

The authors are thankful to the Director of the IUAC, New Delhi, for providing all the necessary facilities to carry out the experiment. One of the authors (AFK) is grateful to Professor Alberto M. Stefanini and Dr. Enrico Fioretto for their helpful discussions with him of the issues and topics addressed by our experiment. One of the authors (AFK) also thanks ICTP/IAEA-INFN for providing him with financial support.

- 
- [1] F. Amorini, M. Cabibbo, G. Cardella, A. Di Pietro, P. Figuera, A. Musumarra, M. Papa, G. Pappalardo, F. Rizzo, and S. Tudsico, *Phys. Rev. C* **58**, 987 (1998).
- [2] M. Cavinato, E. Fabrici, E. Gadioli, E. Gadioli Erba, P. Vergani, M. Crippa, G. Colombo, I. Redaelli, and M. Ripamonti, *Phys. Rev. C* **52**, 2577 (1995).
- [3] P. Vergani, E. Gadioli, E. Vaciago, E. Fabrici, E. Gadioli Erba, M. Galmarini, G. Ciavola, and C. Marchetta, *Phys. Rev. C* **48**, 1815 (1993).
- [4] F. Schussler, H. Nifenecker, B. Jakobsson, V. Kopijar, K. Soderstrom, S. Leray, C. Ngo, S. Souza, J. P. Bondrof, and K. Sneppen, *Nucl. Phys. A* **584**, 704 (1995).
- [5] E. Gadioli, C. Brattari, M. Cavinato, E. Fabrici, E. Gadioli Erba, V. Allori, A. Di. Fillippo, S. Vailati, T. G. Stevens, S. H. Connell, J. P. F. Sellschop, F. M. Nortier, G. F. Steyn, and C. Marchetta, *Nucl. Phys. A* **641**, 271 (1998).
- [6] D. J. Parker, J. J. Hogan, and J. Asher, *Phys. Rev. C* **39**, 2256 (1989).
- [7] D. R. Zolnowski, H. Yamada, S. E. Cala, A. C. Kahler, and T. T. Sugihara, *Phys. Rev. Lett.* **41**, 92 (1978).
- [8] P. P. Singh, B. P. Singh, M. K. Sharma, Unnati, D. P. Singh, R. Prasad, R. Kumar, and K. S. Golda, *Phys. Rev. C* **77**, 014607 (2008).
- [9] P. P. Singh, M. K. Sharma, Unnati, D. P. Singh, R. Kumar, K. S. Golda, B. P. Singh, and R. Prasad, *Eur. Phys. J. A* **34**, 29 (2007).
- [10] D. J. Parker, J. Asher, T. W. Conlon, and I. Naqib, *Phys. Rev. C* **30**, 143 (1984).
- [11] R. S. Siemsen *et al.*, *Nucl. Phys. A* **400**, 245c (1983).
- [12] T. Inamura, M. Ishihara, T. Fakuda, T. Shimoda, and H. Hiruta, *Phys. Lett. B* **68**, 51 (1977).
- [13] M. Blann, *Annu. Rev. Nucl. Sci.* **25**, 123 (1975).
- [14] M. Blann, *Nucl. Phys. A* **235**, 211 (1974).
- [15] C. Signorini *et al.*, *Nucl. Phys. A* **735**, 329 (2004).
- [16] W. Bauer and A. Botvina, *Phys. Rev. C* **52** R1760 (1995).
- [17] A. Corsi *et al.*, *Phys. Lett. B* **679**, 197 (2009).
- [18] B. Fornal *et al.*, *Phys. Rev. C* **42**, 1472 (1990).
- [19] Unnati, P. P. Singh, D. P. Singh, M. K. Sharma, A. Yadav, R. Kumar, B. P. Singh, and R. Prasad, *Nucl. Phys. A* **811**, 77 (2008).
- [20] S. Gupta, B. P. Singh, M. M. Musthafa, H. D. Bhardwaj, and R. Prasad, *Phys. Rev. C* **61**, 064613 (2000).
- [21] M. K. Sharma, B. P. Singh, S. Gupta, M. M. Muthafa, H. D. Bhardwaj, and R. Prasad, *J. Phys. Soc. Jpn* **72**, 1917 (2003).
- [22] M. K. Sharma, Unnati, B. K. Sharma, B. P. Singh, H. D. Bhardwaj, R. Kumar, K. S. Golda, and R. Prasad, *Phys. Rev. C* **70**, 044606 (2004).
- [23] M. K. Sharma, Unnati, B. P. Singh, R. Kumar, K. S. Golda, H. D. Bhardwaj, and R. Prasad, *Nucl. Phys. A* **776**, 83 (2006).
- [24] E. A. Bakkum, P. Decowski, K. A. Griffioen, R. J. Meijer, and R. Kamermans, *Phys. Rev. C* **39**, 2094 (1989).
- [25] J. H. Barker, J. R. Beene, M. L. Halbert, D. C. Hensley, M. Jaaskelainen, D. G. Sarantites, and R. Woodward, *Phys. Rev. Lett.* **45**, 424 (1980).
- [26] N. Wang, X. Wu, Z. Li, M. Liu, and W. Scheid, *Phys. Rev. C* **74**, 044604 (2006).

- [27] S. M. Mullins, A. P. Byrne, G. D. Dracoulis, T. R. McGoram, and W. A. Seale, *Phys. Rev. C* **58**, 831 (1998).
- [28] S. M. Mullins, G. D. Dracoulis, A. P. Byrne, T. R. McGoram, S. Bayer, R. A. Bark, R. T. Newman, W. A. Seale, and F. G. Kondev, *Phys. Rev. C* **61**, 044315 (2000).
- [29] G. J. Lane, G. D. Dracoulis, A. P. Byrne, A. R. Poletti, and T. R. McGoram, *Phys. Rev. C* **60**, 067301 (1999).
- [30] T. Udagawa and T. Tamura, *Phys. Rev. Lett.* **45**, 1311 (1980).
- [31] J. Wilczynski, K. Siwek-Wilczynska, J. Van Driel, S. Gonggrijp, D. C. J. M. Hageman, R. V. F. Janssens, J. Lukasiak, R. H. Siemssen, and S. Y. Van Der Werf, *Nucl. Phys. A* **373**, 109 (1982).
- [32] M. Blann, *Phys. Rev. Lett.* **27**, 337 (1971).
- [33] R. Weiner *et al.*, *Nucl. Phys. A* **286**, 282 (1980).
- [34] J. P. Bondrof, J. N. De, G. Fai, A. O. T. Karvinen, and J. Randrup, *Nucl. Phys. A* **333**, 285 (1980).
- [35] V. I. Zagrebaev, *Ann. Phys. (NY)* **197**, 33 (1990).
- [36] H. Morgenstern, W. Bohne, W. Galster, D. G. Kovar, and H. Lehr, *Phys. Lett. B* **113**, 463 (1982).
- [37] H. Morgenstern, W. Bohne, W. Galster, and K. Grabisch, *Z. Phys. A* **324**, 443 (1986).
- [38] H. Fuchs and K. Mohring, *Rep. Prog. Phys.* **57**, 231 (1994).
- [39] C. Signorini *et al.*, *Phys. Rev. C* **67**, 044607 (2003).
- [40] I. Tserruya, V. Steiner, Z. Fraenkel, P. Jacobs, D. G. Kovar, W. Henning, M. F. Vineyard, and B. G. Glagola., *Phys. Rev. Lett.* **60**, 14 (1988).
- [41] D. J. Parker, J. J. Hogan, and J. Asher, *Phys. Rev. C* **35**, 161 (1987).
- [42] P. E. Hodgson, E. Gadioli, and E. Gadioli Erba, *Introductory Nuclear Physics* (Oxford University Press, London, 1997), Chap. 18.
- [43] *FREEDOM*, *Data acquisition and analysis software*, designed to support accelerator based experiments at the IUAC, New Delhi, India.
- [44] E. Browne and R. B. Firestone, V. S. Shirley, *Table of Radioactive Isotopes* (Wiley, New York, 1986).
- [45] S. Gupta, B. P. Singh, M. M. Musthafa, H. D. Bhardwaj, and R. Prasad, *Phys. Rev. C* **61**, 64613 (2000).
- [46] Avinash Agarwal, I. A. Rizvi, Rakesh Kumar, B. K. Yogi, and A. K. Chaubey, *Int. J. Mod. Phys. E* **17**, 393 (2008).
- [47] S. F. Mughabghab, M. Divadeenam, and N. E. Holden, *Neutron Cross-Sections* (Academic Press, New York, 1981), Vol. 1, Part A, p. 89.
- [48] A. Gavron, *Phys. Rev. C* **21**, 230 (1980).
- [49] F. D. Becchetti and G. W. Greenless, *Phys. Rev.* **182**, 1190 (1969).
- [50] G. R. Satchler, *Nucl. Phys.* **70**, 177 (1965).
- [51] J. R. Huizeya and G. Igo, *Nucl. Phys.* **29**, 462 (1962).
- [52] R. Bass, *Nucl. Phys. A* **231**, 45 (1974).
- [53] J. K. Tuli, *Nuclear Wallet Card*, National Nuclear Data Center, Brookhaven National Laboratory, Upton, NY, 2000.
- [54] M. Blann, *NEA Data Bank*, Gif-sur-Yvette, France, Report PSR-146, 1991.
- [55] V. Weisskopf, *Phys. Rev.* **52**, 295 (1937).
- [56] J. Wilczynski, *Nucl. Phys. A* **216**, 386 (1973).
- [57] H. Morgenstern, W. Bohne, W. Galster, K. Grabisch, and A. Kyanowski, *Phys. Rev. Lett.* **52**, 1104 (1984).